Nanostructures from nanoparticles

2003 J. Phys.: Condens. Matter 15 S3047

(http://iopscience.iop.org/0953-8984/15/42/005)

INSTITUTE OF PHYSICS PUBLISHING JOURNAL OF PHYSICS: CONDENSED MATTER

J. Phys.: Condens. Matter **15** (2003) S3047–S3063 PII: S0953-8984(03)65824-8

Nanostructures from nanoparticles

Paula M Mendes[1], Yu Chen[2], Richard E Palmer[2], Kirill Nikitin[3], Donald Fitzmaurice[3] and Jon A Preece[1,4]

[1] School of Chemical Sciences, University of Birmingham, Edgbaston, Birmingham B15 2TT, UK
[2] Nanoscale Physics Research Laboratory, School of Physics and Astronomy, University of Birmingham, Edgbaston, Birmingham B15 2TT, UK
[3] Nanochemistry Group, Department of Chemistry, University College Dublin, Belfield, Dublin 4, Republic of Ireland

E-mail: j.a.preece@bham.ac.uk

Received 8 July 2003
Published 10 October 2003
Online at stacks.iop.org/JPhysCM/15/S3047

Abstract

This paper reviews recent experimental approaches to the development of surface nanostructures from nanoparticles. The formation of nanowires by electron beam writing in films of gold nanoparticles passivated with a specially designed class of ligand molecules (dialkyl sulfides) is presented, together with illustrations of practical nanostructures. Potential applications of this methodology are discussed. Another alternative to the controlled fabrication of arrays of nanoparticles, based on nanocrystals which contain molecular recognition elements in the ligand shell, is also surveyed. These particles aggregate in the presence of specifically designed molecular dications which act as a molecular binder. Finally, recent work on the formation of nanoscale surface architectures using x-ray patterning of self-assembled monolayers is introduced. Current and potential future applications of these surface nanostructures are discussed.

(Some figures in this article are in colour only in the electronic version)

1. Introduction

Precise control of the structure of matter at the nanometre scale may have revolutionary consequences for science and technology. The ability to assemble nanoparticles into arrays, networks and circuits in a precise and controlled manner represents the key to the fabrication of a variety of nanodevices. Networks of nanometre-sized metal or semiconductor islands, or quantum dots, may exhibit a variety of quantum phenomena, with potential applications

[4] Author to whom any correspondence should be addressed.

in optical devices, nanometre scale sensors, advanced computer architectures, ultra-dense memories and quantum-information processing.

The fabrication of nanoparticle arrays with nanoscale precision in a time- and cost-effective manner remains a formidable task. While the traditional semiconductor fabrication approach is based on 'top-down' techniques, i.e. lithography [1, 2], and the construction of nanostructures via the assembly of molecular-sized components, the so-called 'bottom-up' chemical approach may in the future offer a number of potentially very attractive advantages. These include experimental simplicity down to the atomic size scale, the possibility of three-dimensional assembly and the potential for low-cost mass fabrication. Moreover, these technological prospects notwithstanding, a major motivation for research in this field remains the challenge to understand how ordered or complex structures form spontaneously by self-assembly, and how such processes can be controlled in order to prepare structures with a pre-determined geometry. In this paper, we review progress that we have made [3–7] in developing methods for producing nanostructures from metal nanoparticles. Three main approaches are discussed. One is the formation of nanowires by direct electron beam writing in Au films passivated with organic ligands, including novel ligands such as dialkyl sulfides [3, 4]. Demonstrations of nanostructure fabrication by this method on practical Si/SiO_2 surfaces are also given. The generation, or programmed assembly, of complex nanocrystal architectures in solution provides an alternative method of forming nanostructures from nanoparticles. Silver nanocrystals stabilized by a mixture of chemisorbed alkanethiol (85%) and similar molecules incorporating a molecular recognition group are shown to undergo chemical assembly. The third approach described to nanostructure fabrication is the chemical modification of self-assembled monolayers (SAMs) by x-ray irradiation (nitro to amine group conversion) [7]. This method promises to produce chemically patterned surfaces for selective nanoparticle attachment. Together these three approaches represent a toolbox for the fabrication of novel nanometre scale architectures on surfaces.

2. Fabrication of metallic nanostructures by direct electron beam writing on nanoparticle films

Nanoparticles stabilized by organic ligands have attracted considerable interest because of their potential as 'artificial atoms' from which to assemble nanoscale structures and devices [8–18]. Such assemblies can also be subjected to further processing by lithographic techniques. For example, organic ligands such as alkanethiol molecules, which prevent aggregation of metal nanoparticles when they are adsorbed on the surface, can be fragmented by direct electron irradiation [19–23]. This technique has the potential to reduce the fabrication of metallic nanostructures to a three-step process: coating, writing and rinsing, as shown in scheme 1. In principle, it may be possible to fabricate structures as small as the nanoparticle core size, i.e. 1–10 nm. The technique may therefore allow us to make nanoscale wires to link components within or between nanoscale devices and to connect such devices to the macroscopic world, addressing two of the key challenges in nanotechnology [24].

Ideally, such nanoscale connections should show very good electrical conductivity. The ratio of metal to non-metallic atoms in passivated nanoclusters is much higher than in more conventional organometallics, such as ferrocene, $(C_5H_5)_2Fe$, which have also been employed in electron beam writing [25]. It was found that electron irradiation of alkanethiol monolayers self-assembled on a Au(111) surface leads mostly to cleavage of the C–H and C–C bonds [19–21]—approximately 60% of the original Au–thiolate bonds remain after an electron dose of 1000 $\mu C\,cm^{-2}$ [22]. Coexistence of alkanethiols and irradiation-induced species was observed by high resolution x-ray photoelectron spectroscopy (XPS) of strongly irradiated

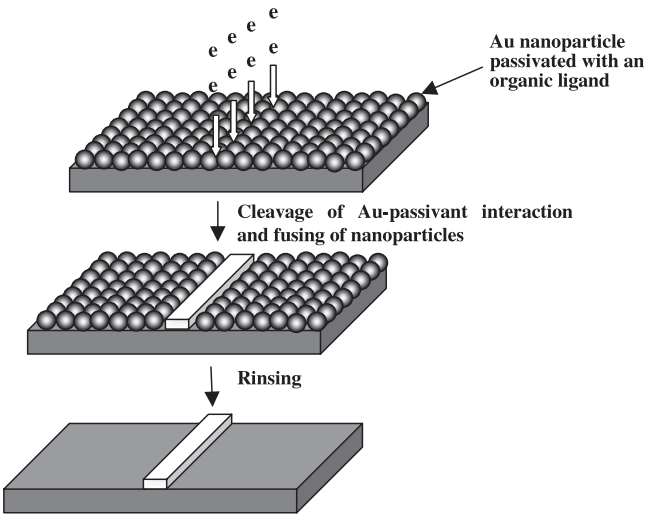

Scheme 1. Fabrication of gold-based wires by electron beam writing in films of passivated gold nanoparticles.

$C_{12}H_{25}SH$ SAMs on Au surfaces [23]. Thus a certain amount of residual carbon contamination seems inevitable in electron beam writing in films of nanoparticles passivated with alkanethiol molecules and this will affect the conductivity of the nanostructures produced. Therefore, new types of ligands are needed to optimize the direct electron beam writing technique by minimizing the amount of carbon contamination in the resulting nanoscale structures.

Dialkyl sulfide ligands are good candidates for the efficient cleavage of Au–S bonds. The strength of the Au–S bond for SAMs formed from dialkyl sulfides is 60 kJ mol^{-1}, whereas the Au–S bond for SAMs formed from alkanethiols has a strength of 126 kJ mol^{-1} [26]. In addition to a weaker Au–S bond, dialkyl sulfides (RSR′) present other potential advantages over thiols (RSH) and dialkyl disulfides (RSSR′) as passivants: (i) R and R′ can be varied independently and with ease and (ii) the issue of phase separation [27] when SAMs are formed from dialkyl disulfides or binary solutions of thiols is eliminated.

Despite extensive investigations of SAMs of dialkyl sulfides on planar gold surfaces [28], there are only a few studies of dialkyl sulfides as passivants for gold nanoparticles [3, 29–31]. In our work [3], gold nanoparticles passivated with didecyl sulfide ($H_{21}C_{10}SC_{10}H_{21}$) were synthesized via the borohydride reduction of $HAuCl_4$ [32] and characterized by ^{1}H NMR, FTIR, UV–vis, Auger electron spectroscopy, XPS and transmission electron spectroscopy (TEM). For meaningful comparison, decanethiol ($C_{10}H_{21}SH$) passivated nanoparticles were also prepared in an identical way to the dialkyl sulfide passivated nanoparticles.

UV–vis spectra of gold colloids stabilized by didecyl sulfide showed broad UV absorption bands around 520 nm, corresponding to nanoparticles in the 5–6 nm size range. Analysis of the TEM micrographs of the nanoparticles was in agreement with these results (figure 1). From the analysis of the images, the average diameter of gold particles passivated with $H_{21}C_{10}SC_{10}H_{21}$ was 5.3 ± 0.8 nm. However, under equivalent conditions of formation, the size and polydispersity of the gold cores obtained are greater for the didecyl sulfide ligands than decanethiol ligands; in the latter case the nanoparticles were 2.2 ± 0.1 nm in diameter.

To further characterize the passivated gold nanoparticles, the samples were analysed by XPS measurements. The XPS survey spectra of the nanoparticles assembled on graphite showed O (1s), Au (4f), Au (4d), Au (4p) and C (1s) signals, with a weak S (2p) peak

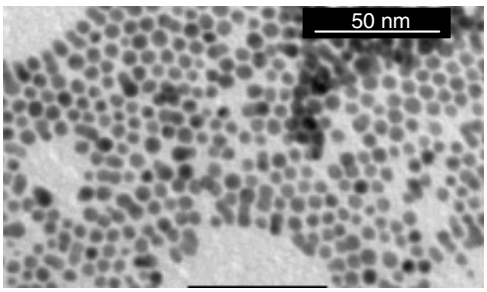

Figure 1. TEM micrograph of $H_{21}C_{10}SC_{10}H_{21}$ passivated gold nanoparticles, from [3].

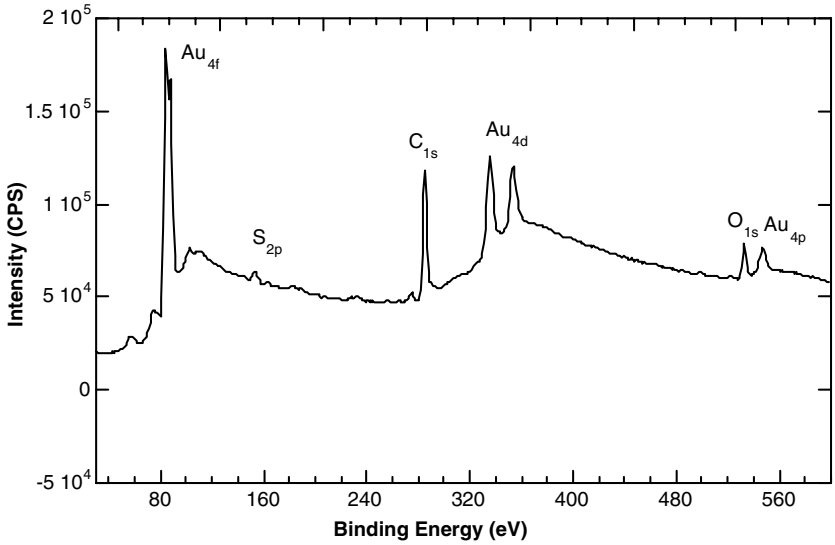

Figure 2. XPS survey spectra of the $H_{21}C_{10}SC_{10}H_{21}$ passivated gold nanoparticles (the binding energies are referenced to the Au ($4f_{7/2}$) line at 84 eV), from [3].

(figure 2). The presence of the O (1s) peak (533 eV) suggests oxidation of the organic ligands/nanoparticles, including R_2SO (∼531.6 eV) and R_2SO_2 (∼531.8 eV) species in the film. It is worth noting that the presence of H_2O (∼532.9 eV) could also contribute to the O (1s) peak. High resolution electron energy loss spectroscopy (HREELS) was also employed to study the films of gold nanoparticles passivated with dialkyl sulfide ligands on graphite [4]. Energy loss peaks due to CH_x and C–C vibrational modes of the organic ligands were observed, together with a peak at 230 cm^{-1} assigned to the Au–S stretching mode (figure 3(a)).

In order to explore the response of the nanocluster film to electron beam irradiation, the film was exposed to a prolonged period of low energy electron irradiation at 50 eV [4]. After electron beam irradiation for a total dosage of approximately 90 μC over a ∼5 mm spot size (∼360 μC cm^{-2}) significant changes were found in the HREEL spectra, figure 3(b). The 230 cm^{-1} mode (Au–S stretch) diminished significantly and a new feature at 460 cm^{-1} appeared, indicating cleavage of the Au–S bond and, possibly, the formation of sulfoxides. These results raise the possibility of fabricating nanowires to link nanoscale components and devices by direct electron beam writing in the dialkyl sulfide–gold systems.

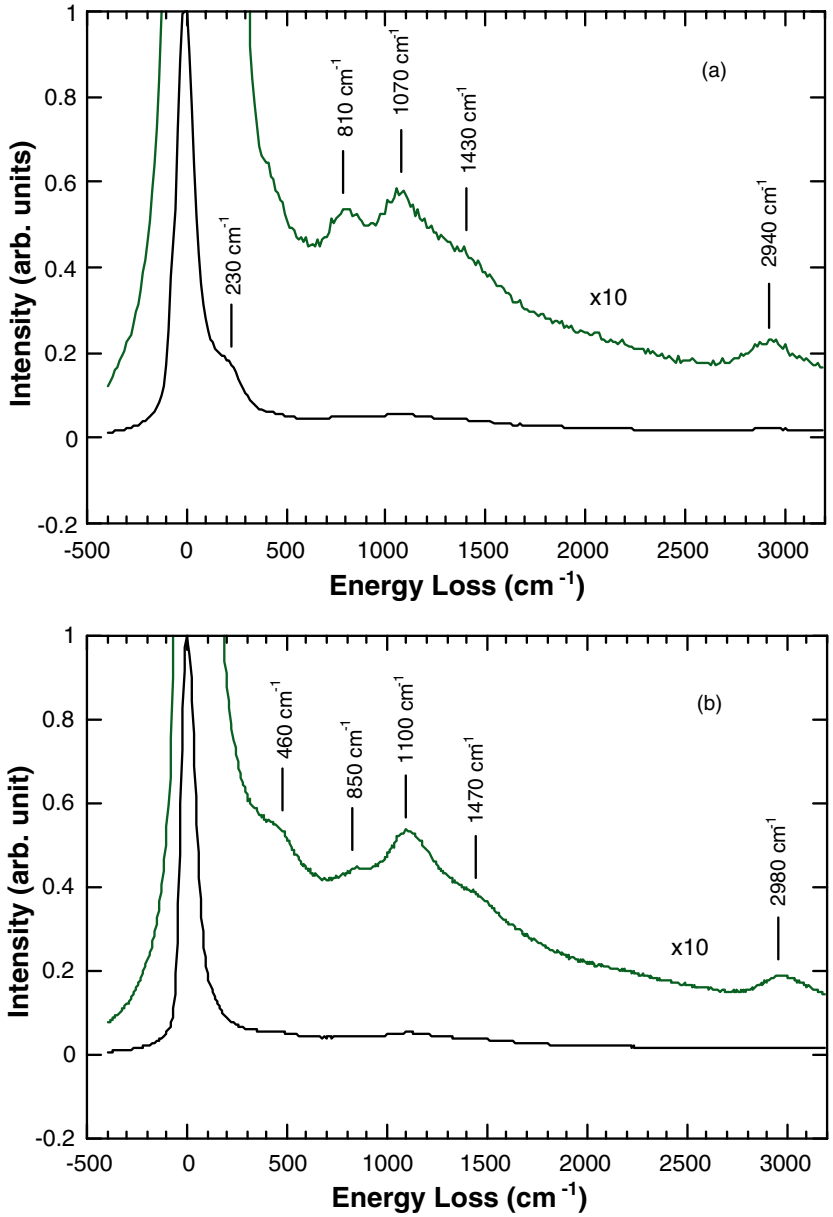

Figure 3. (a) A typical HREELS spectrum from a film of dialkyl sulfide ($H_{21}C_{10}SC_{10}H_{21}$) passivated gold nanoparticles on graphite. Incident electron energy 4.5 eV; incident angle 60°; specular scattering geometry. (b) HREELS spectrum taken after the film was exposed to a low energy electron dosage of approximately 90 μC at 50 eV. Scattering conditions as for (a), from [4].

Figure 4(a) illustrates the results of direct electron beam writing in the dialkyl sulfide passivated gold nanoparticles on a thermally grown SiO_2 film (thickness 65 nm) on a Si wafer at different dosages with a beam energy of 6 keV. The lines are 1.7 μm long and 200 nm apart. It was found that the linewidth increases with increasing electron dose. The

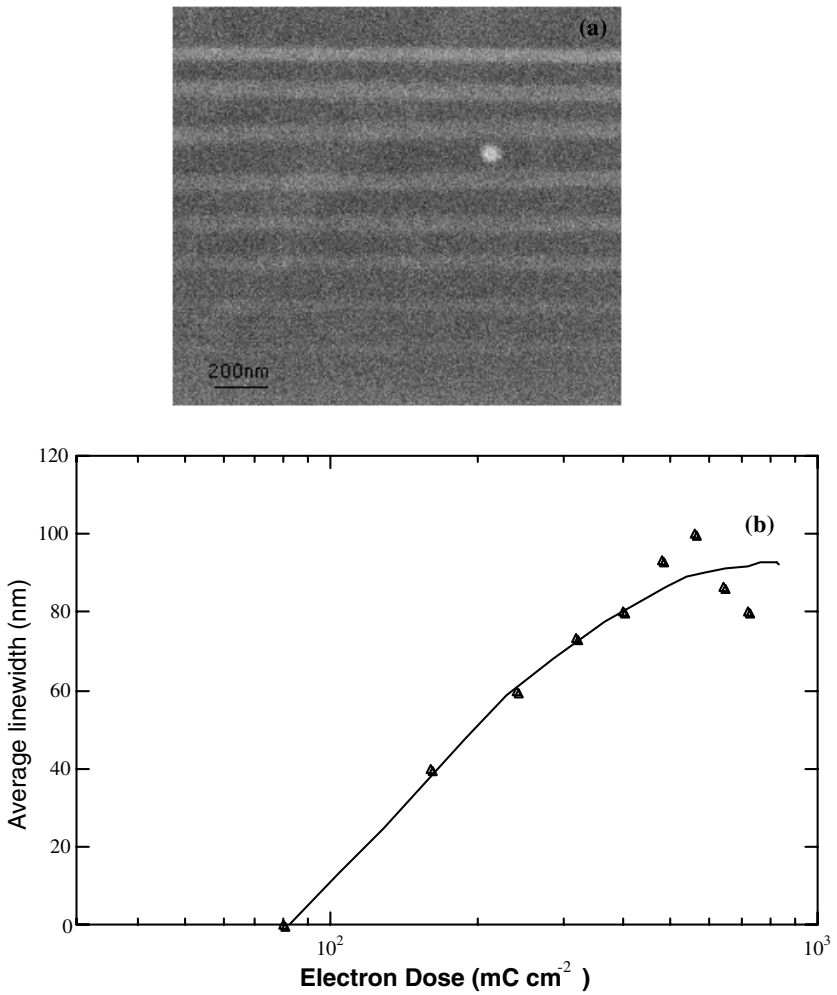

Figure 4. (a) SEM image of direct electron beam writing in the dialkyl sulfide passivated gold nanoparticles. (b) Response curve for a film of dialkyl sulfide passivated gold nanoparticles on thermally grown SiO_2 film (thickness 65 nm) on a Si wafer. Shown is the width of the lines produced by direct electron beam writing at 6 keV as a function of electron dose.

average linewidth of the bottom line (the narrowest) is about 40 nm and was generated with a dose of 160 mC cm^{-2}. A response curve, which plots the linewidth as a function of electron beam dose as shown in figure 4(b), provides a practical, quantitative measure of the sensitivity of the nanoparticle film. If we describe the sensitivity of the nanoparticle film by the threshold dose for production of exposed lines visible in the SEM, then a sensitivity of 80 mC cm^{-2} is derived. This value suggests that the nanoparticle film is about 600 times less sensitive in comparison with PMMA (quoted as 0.13 mC cm^{-2}) [33]. However, this sensitivity lies at present within an order of magnitude or so of other high resolution negative tone electron beam resists, e.g. calixarene MC6AOAC (7 mC cm^{-2}) [34], C60 (10 C cm^{-2}) [35], hexapentyloxytriphenylene (2.5 mC cm^{-2}) [36] and alkanethiol passivated nanoparticles (5.4 mC cm^{-2}) [37].

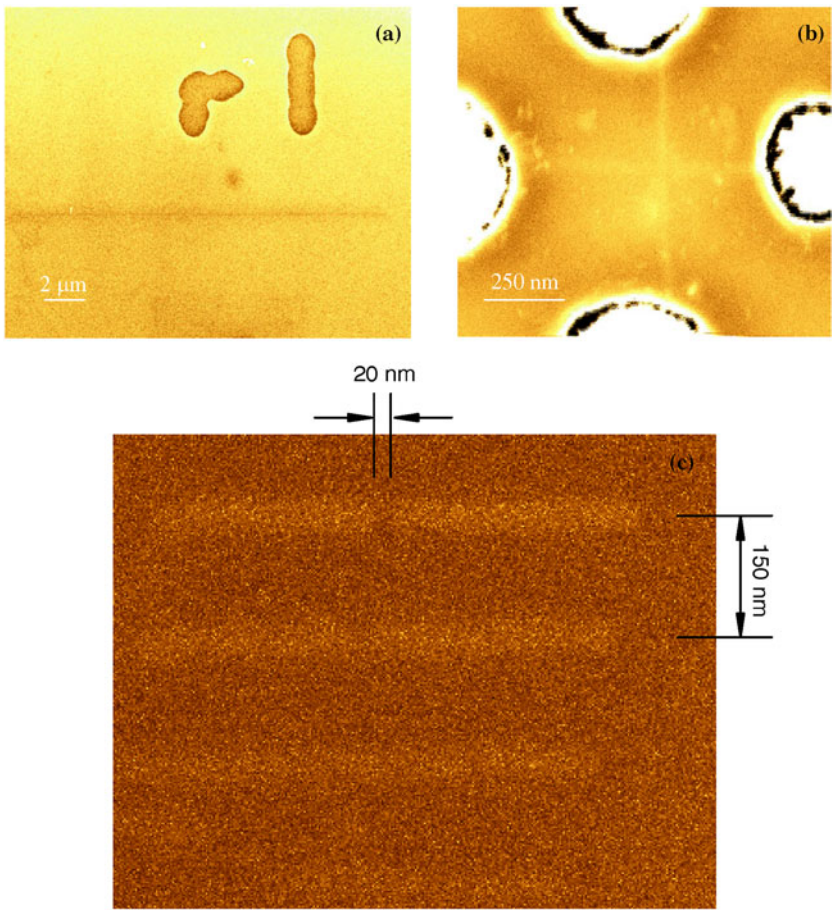

Figure 5. SEM images demonstrating direct electron beam writing in nanoparticle films. (a) A line 20 μm long and 40–50 nm wide produced in a film of alkanethiol passivated gold nanoparticles on a thermal SiO_2 substrate (electron beam energy 7 keV; dose 50×10^3 μC cm^{-2}). (b) Perpendicular nanowires connecting two pairs of Au electrodes prefabricated by photolithography. (c) Parallel lines produced in a film of dialkyl sulfide passivated gold nanoparticles on a thermal SiO_2 substrate. The top wire exhibits a small gap (∼20 nm as labelled).

3. Electron beam writing in nanoparticle films of silicon

As discussed in the previous section, direct electron beam writing in films of passivated nanoparticles can be employed to create nanoscale features on surfaces. Indeed, wires with widths down to 26 nm have been produced [37]. Here, we illustrate the potential applications of the direct electron beam writing technique, with particular reference to the technologically important Si/SiO_2 surface. Figure 5(a) illustrates the fabrication of individual wires via direct electron beam writing in a thin film of alkanethiol passivated Au nanoparticles on a Si substrate terminated by a thermally grown SiO_2 layer. The nanoparticle film was formed by insertion of the substrate into the nanoparticle solution for 1 day. An electron beam energy of 7 keV was employed, with a probe size of about 10 nm. The designed pattern is a line one pixel wide and 20 μm long. A typical line, 20 μm long but only 40–50 nm wide, i.e. with an aspect ratio of about 400:1, was created with a dose of 10 mC cm^{-2} as shown in figure 5(a) (above the line is an alignment mark designed for further photolithographic processing). Nanowires as long

as 60 μm have been fabricated using this technique. Success in obtaining long lines depends mainly on the quality of the nanoparticle film. Large voids in the film naturally result in a discontinuous line.

Figure 5(b) shows that the direct electron beam writing technique is also compatible with conventional lithography, thus enabling the creation of nanoscale structures on pre-patterned surfaces. Figure 5(b) shows a cross formed by two nanowires ($\sim$30 nm wide), each of which bridges a pair of metal electrodes, $\sim$750 nm apart, prefabricated on Si/SiO_2 substrate via conventional photolithography. In this case, the vertical line was written after the horizontal one by rotating the sample by 90°. The alignment was achieved directly via SEM imaging, which is a benefit of the relatively low electron beam sensitivity of the nanoparticle film, i.e. about 80 times less than PMMA. Wires 40 μm in length and with an average width of approximately 70 nm running across four parallel gold microelectrodes with 5 μm gaps (for conductivity measurements) have also been generated by this technique. Again, the success of this 'wire on pattern' strategy demands a good quality nanoparticle film over the whole patterned area, which remains a challenge on surfaces with deep and/or complex features. Further investigations are required to optimize the coating techniques.

One potential application of nanoscale wires is to make electrical contacts to nanometre-scale objects, e.g. nanoparticles or molecules. The creation of a gap structure provides a template for the incorporation of a molecule or nanoparticle whose transport properties are to be explored. In recent years, a number of techniques have been developed to fabricate small gaps between two electrodes, including shadow deposition [38], electrochemical deposition [39], electromigration [40], scanning probe lithography [41] and controlled electron beam lithography [42]. Direct electron beam writing can also create such gaps, as figure 5(c) illustrates. A thin film of gold nanoparticles passivated with dialkyl sulfide ligands ($C_{10}H_{21}SC_{10}H_{21}$), of the kind discussed above, was formed on a Si substrate with a thermally grown SiO_2 layer and subsequently exposed to a 6 keV electron beam. The designed pattern consists of four lines with 150 nm separation and a gap in the middle. The designed gap sizes are 5, 10, 15 and 20 nm running from bottom to top in figure 5(c). A definite gap of size $\sim$20 nm is visible in the top line. The resolution (about 20 nm in this case) is probably limited by the beam size and by proximity, i.e. the electron scattering effect [43]. It is possible that the gap can be further narrowed via proximity effect correction [44].

4. Chemical assembly of nanocrystals

Size-monodisperse nanocrystals of a wide range of materials have been prepared and their size-dependent electronic and magnetic properties studied [45–53]. However, it is the collective electronic and magnetic properties of organized assemblies of size-monodisperse nanocrystals that are increasingly the subjects of investigation [45, 47, 49, 54–58]. Interest in these organized assemblies is enhanced by the fact that it ought to be possible to fine-tune their properties by controlling the size of constituent nanocrystals. The findings of these and related investigations suggest that it may be possible to self-assemble complex nanocrystal architectures in solution or on a substrate.

Generally, organized assemblies of nanocrystals are prepared at an air–water interface (two-dimensional) [56] or on a suitable substrate by controlled solvent evaporation (three-dimensional) [54]. However, both approaches are limited by the fact that only relatively simple nanocrystal architectures can be realized. For this reason, strategies that permit the assembly of complex nanocrystal architectures are of particular interest.

One strategy is to prepare a dispersion of nanocrystals stabilized by molecules incorporating one or more binding sites. These binding sites should serve to define uniquely

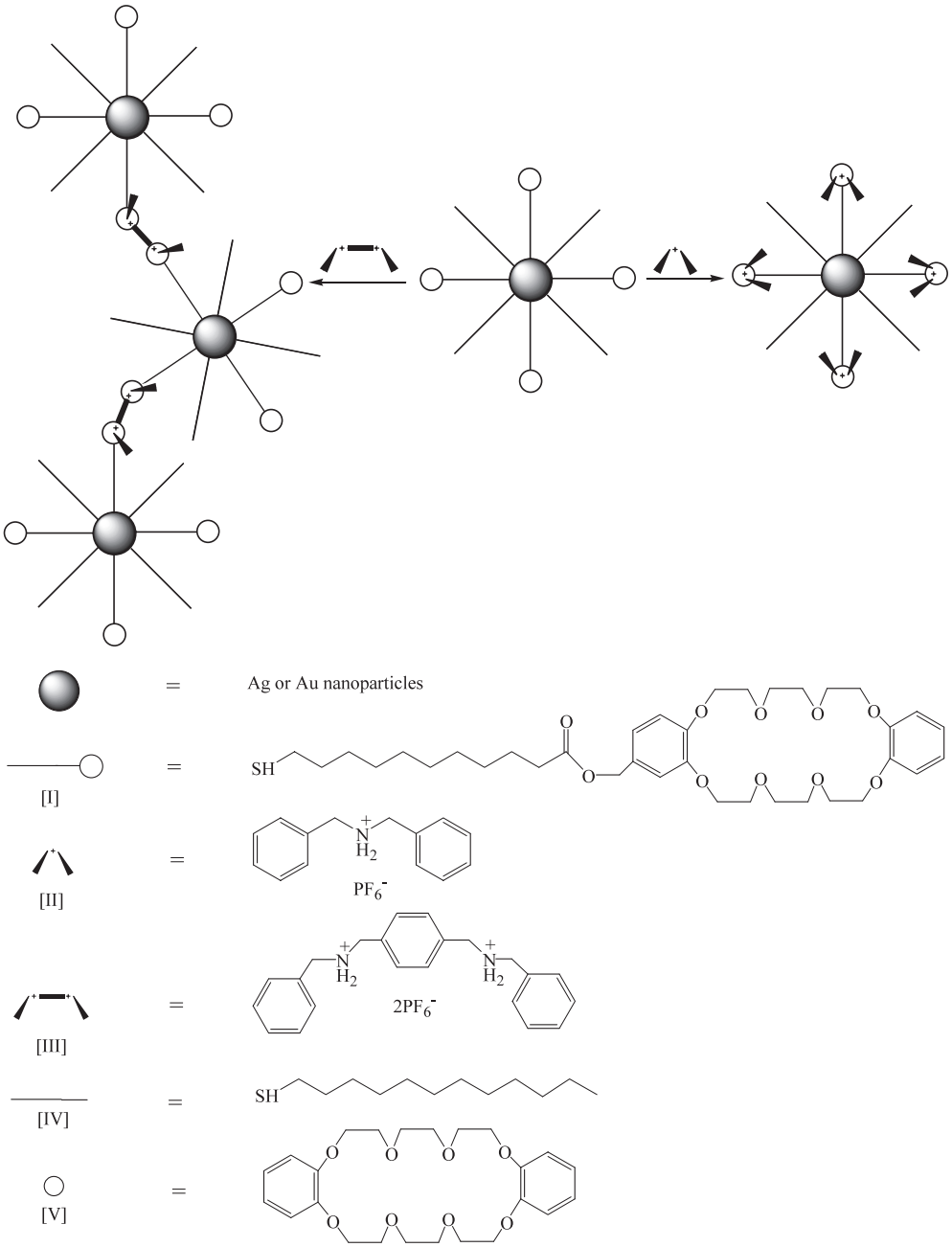

Scheme 2. Formation of pseudorotaxanes on a single crystal (right) and bridging two different crystals inducing nanocrystal aggregation (left).

the position of a nanocrystal in the architecture to be assembled. Upon mixing a number of such dispersions, each nanocrystal should recognize and bind a nanocrystal from another dispersion or a well-defined region on the surface of a suitably patterned substrate. By this means, it should be possible to programme the parallel assembly of identical multiple copies of the desired nanocrystal architecture in solution or on a substrate.

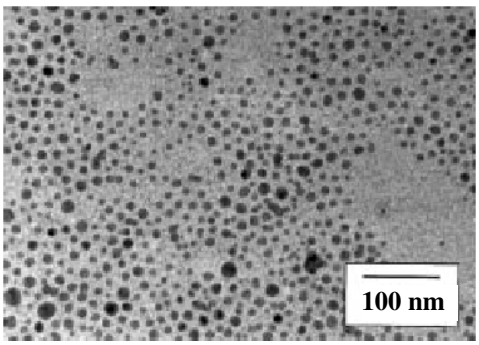

Figure 6. TEM picture of gold nanocrystals stabilized by a chemisorbed monolayer of I (Au–I), from [5].

As a first step, a dispersion of gold nanocrystals possessing a narrow size distribution and stabilized by a chemisorbed monolayer of a undecane thiol derivative covalently linked to dibenzo[24]-crown-8 (I) was prepared and characterized, as shown in scheme 2 [5]. TEM establishes that the average diameter of a gold nanocrystal in Au–I is 4.2 ± 0.8 nm (figure 6). Elemental analysis establishes that the average number of I adsorbed at the surface of each nanocrystal is 300. On this basis, it has been calculated that the average surface area occupied by each molecule I is 1.8 nm^2. This value is smaller than that for a monolayer of I self-assembled at a planar gold substrate (2.1 nm^2) [59], but, as expected, somewhat larger than that reported for an alkanethiol adsorbed at the surface of a gold nanocrystal (1.6 nm^2) [60]. These findings can be explained by the extreme curvature of the gold nanocrystal and the steric hindrance associated with the terminal crown moiety of I, respectively.

It was expected that these nanocrystals, denoted Au–I, would recognize and bind selectively the dibenzylammonium cation (II) in solution to form the pseudorotaxane (scheme 2). In fact, quantitative analysis of ^{1}H NMR of an equimolar mixture of Au–I and II indicates that 86% of the dibenzo[24]-crown-8 binding sites at the surface of each gold nanocrystal in Au–I are complexed with a dibenzylammonium cation (II). However, as II contains only one binding site this recognition event does not lead to aggregation of nanoparticles.

In the case of the bis-dibenzylammonium dication (III), there is the possibility of bridging two nanocrystals and of aggregation (scheme 2). For this purpose, near size-monodisperse silver nanocrystals, stabilized by chemisorption of a mixture of 85% of an alkane thiol (IV) and 15% of an alkane thiol covalently linked to a dibenzo[24]-crown-8 moiety (I) were synthesized [6]. One possible route for its synthesis is to prepare silver nanocrystals in the presence of a mixture of IV and I. However, nucleation of nanocrystals in the presence of a mixture of thiols generally leads to irregularly shaped clusters that are not amenable to size-selective precipitation [61]. As a consequence, the approach adopted was similar to that developed by Murray and co-workers [61], i.e. surface exchange between an adsorbed thiol and a thiol incorporating a binding site in solution.

The TEM image (figure 7(a)) demonstrated that modification of Ag–IV to form Ag–IV/I does not result in a significant change in the diameter or the degree of polydispersity of the silver nanocrystals. Specifically, an analysis of 200 nanocrystals yields an average diameter for the silver nanocrystal core of 7.3 ± 0.8 nm and a polydispersity of 1.09. These values agree well with those obtained for Ag–IV. Analysis of the ^{1}H NMR spectrum confirms that molecules IV and I are chemisorbed at the surface of the Ag nanocrystal. Elemental analysis estimates the organic composition to be 17.6%. Assuming the nanocrystals are spherical and

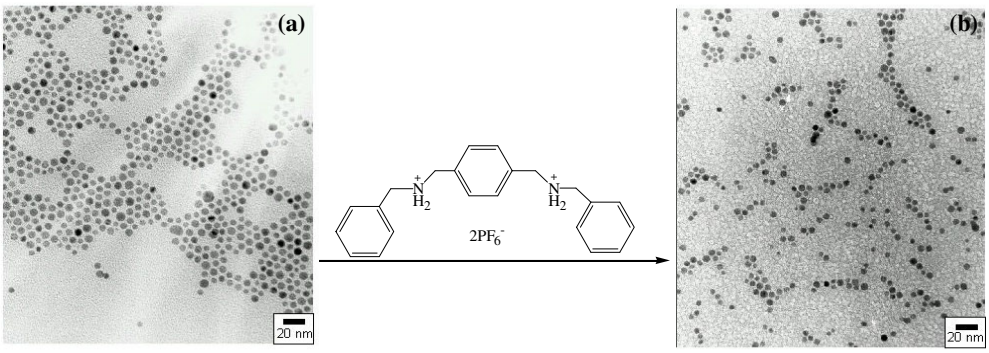

Figure 7. TEM picture of silver nanocrystals stabilized by a chemisorbed monolayer of IV (85%) and I (15%) (a) prior to and (b) following addition of III.

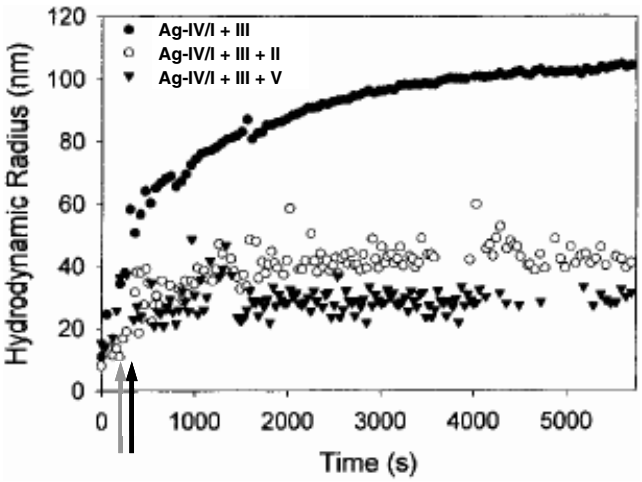

Figure 8. DLS profiles of Ag–IV/I, prior to and following addition of III. Also plotted are DLS profiles prior to and following addition of III and subsequent addition of II or V. The arrows indicate the time of addition of II (dark grey) and V (light grey), from [6].

covered by a monolayer of IV and I, it has been calculated that each nanocrystal is covered by an average of 1015 thiol molecules (152 molecules of I, assuming 15% coverage as determined from the ^{1}H NMR spectrum) and that each thiol occupies on average 1.7 nm^2 of the available surface area [62]. This value is significantly larger than that for Ag–IV due, possibly, to the steric bulk associated with the dibenzo[24]-crown-8 moiety.

Shown in figure 8 are dynamic light scattering (DLS) measurements made following addition of III, dissolved in MeCN, to Ag–IV/I dispersed in $CHCl_3$ (2:1 ratio of IV/I and III). It is clear from these measurements that addition of III is followed by a growth in the hydrodynamic radius of the scattering entity which, based on the findings reported above, is assumed to be silver nanocrystal aggregates of the type shown in scheme 2. The growth of the aggregate in solution is power law in nature and suggests strongly that aggregation is diffusion-limited and that the aggregates formed are open fractal structures [63].

If pseudorotaxane formation is the driving aggregation then it would be expected that aggregation of Ag–IV/I, in the presence of III, would be inhibited by addition of an excess of II or V. From figure 8 it is clear that complete inhibition of further growth occurs after addition

of II and V to an aggregating colloid of Ag–IV/I. In the case of the addition of an excess of II, the available binding sites on the surface of Ag–IV/I were occupied and, therefore, incapable of binding to another Ag–IV/I. In the case of the addition of an excess of V, the unbound III present in solution was complexed and was no longer able to participate in nanocrystal aggregation.

Since pseudorotaxane formation between the molecular components, III and V, is a molecular interaction, it occurs on a timescale shorter than that for pseudorotaxane-driven nanocrystal aggregation between Ag–IV/I and III. This is shown by the rapid quenching of further growth upon the addition of inhibiting compounds, i.e. a reaction where rate is dependent on the diffusion of molecules to binding sites situated on nanocrystals.

It was interesting to note that, upon TEM characterization of a solution of Ag–IV/I and III dropped onto a copper grid and the solvent evaporating, no longer were the particles aggregated as in figure 7(a) but were forming narrow aggregates (figure 7(b)) and, in some cases, linear arrays of nanoparticles. This result was of some surprise initially, as the solution data suggest greater aggregation. However, the aggregation in solution was thought to be fractal in nature. We presume that open fractal aggregation is a result of the repulsive interaction of the dications linking the nanoparticles, which lives on during the nanoparticle assembly on the TEM grid. The ability to control the extent of aggregation is a novel feature and points towards future developments in controlling nanocrystal assembly.

5. X-ray irradiation as a tool for patterning SAMs

The self-assembly of complex nanocrystal architectures in solution has been discussed in the previous section. Another intriguing route for the formation of nanostructures is the use of surface templates onto which the particles can assemble in a pre-determined fashion [64]. Patterning of SAMs is a particularly promising process for preparing such templates [1, 65–71]. SAMs are homogeneous, highly ordered films which can possess variable surface chemical properties [72, 73]. Direct chemical synthesis of nanostructures on a patterned solid template that is capable of defining the position and lateral dimensions of the objects to be grown offers a suitable route for the generation, precise positioning, spatial fixation and lateral interaction of various types of nanoparticles of interest.

Patterning SAMs can be achieved using a variety of techniques, which includes UV photopatterning [1], microcontact printing [66], electron beam lithography [67, 71] and scanning probe microscopy (SPM) based techniques such as ‘dip-pen nanolithography’ [68], ‘nanografting’ and ‘nanoshaving’ [69].

Although XPS has been widely used to obtain information on the formation and composition of films, several studies have demonstrated that x-rays induce damage and modification of SAMs [71, 74–81]. This damage can either limit the utility of x-ray irradiation or be used as a lithographic approach to pattern surfaces [70].

Kim and co-workers [65] studied visible laser light irradiation effects on nitro-terminated monolayers on silver. The results indicated the conversion of the nitro group to amine functionality by laser irradiation, preserving the overall structural integrity of the monolayer. Grunze and co-workers [71] investigated NO_2-terminated biphenyl SAMs on gold substrates. They reported the transformation of surface nitro groups to amine groups by low energy electron irradiation while the underlying aromatic layer is dehydrogenated and cross-linked. They suggested that the hydrogen atoms required for reduction of the nitro groups are generated by the electron-induced dissociation of the C–H bonds in the biphenyl units.

Taking into consideration these previous studies, we carried out research on the influence of x-ray irradiation on a similar system (scheme 3) [7]. In order to investigate whether the

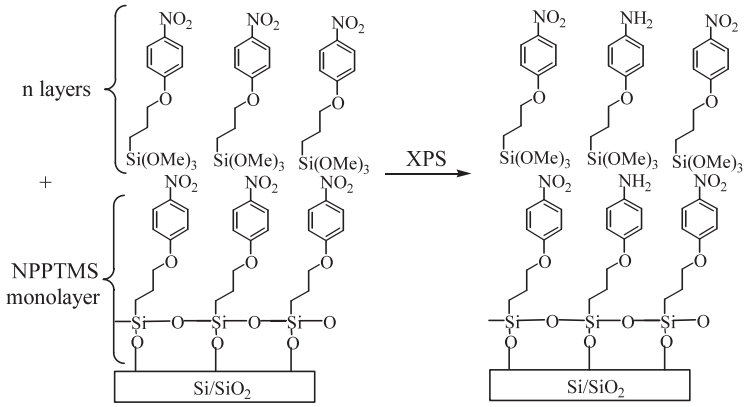

Scheme 3. Schematic representation of the formation and modification of multilayers of self-assembling silanes, with NPPTMS as the basic monolayer building unit.

XP source can be used to chemically modify the NO_2 moiety to NH_2 moiety, we synthesized 3-(4-nitrophenoxy)-propyltrimethoxysilane (NPPTMS).

Due to the low signal intensity of the elements in SAMs during XPS analysis, prolonged acquisition times are required in order to obtain a higher signal-to-noise ratio. However, during this extended period of measurement molecular components of SAMs may undergo substantial chemical and structural transformations as a result of the irradiation. Therefore, as a first step in our study for demonstrating the conversion of the NO_2 to the NH_2 group of organic thin films on silicon by XPS irradiation, we formed multilayer films of NPPTMS with subsequent enhanced resolution of binding energy peaks, compared with ultra-thin films (e.g. SAMs), i.e. higher signal-to-noise for shorter XP exposure times.

Organic films were prepared by immersing Si/SiO_2 substrates in a solution of NPPTMS in anhydrous $CHCl_3$ for 2 h. Ellipsometry showed that the average film thickness was 2.7 ± 0.2 nm.

NPPTMS multilayer films were then exposed to x-ray irradiation (Mg Kα at 1253.6 eV source) for 447 min, collecting data every 6 min. Results from the XPS elemental composition data suggested chemical modification of the NO_2 group. Clearly, the spectrum presented in figure 9(a) (3 min) shows the N (1s) binding energy at 405.6 eV, characteristic of the NO_2 moiety (literature 405.5 eV) [82, 83]. As time progresses, a second peak at 399.6 eV appears, which would correspond to the binding energy of an NH_2 functionality (lit. 399 eV) [82, 83]. Furthermore, the spectra represented in figures 9(a)–(e) at different irradiation times of 3, 97, 163, 273 and 447 min show the decrease in the peak intensity of the N (1s) binding energy of the NO_2 group with the concomitant increase of the peak area of N (1s) binding energy at 399.6 eV[5]. At longer irradiation times (447 min), almost all NO_2 groups under irradiation were converted to NH_2 groups (figure 9(e)).

Figure 10 shows the evolution of the N (1s) peak area for NH_2, NO_2 and NH_2+NO_2 within the film as a function of x-ray exposure time. It should be noted that the total nitrogen peak area (NO_2 and NH_2 regions) appears to decrease slightly with prolonged irradiation times (by 18% after 447 min continuous irradiation), suggesting irradiation-induced partial desorption of N-containing molecular fragments. No significant changes were observed on O (1s), C (1s) and

[5] As an aside, we have assigned the N (1s) peak at 399.6 as the NH_2 functionality, but it is worth noting that this peak can be deconvoluted into two different nitrogen species at 399.3 and 400.8 eV, which are characteristic of an amine and a protonated amine group (ammonium), respectively [81].

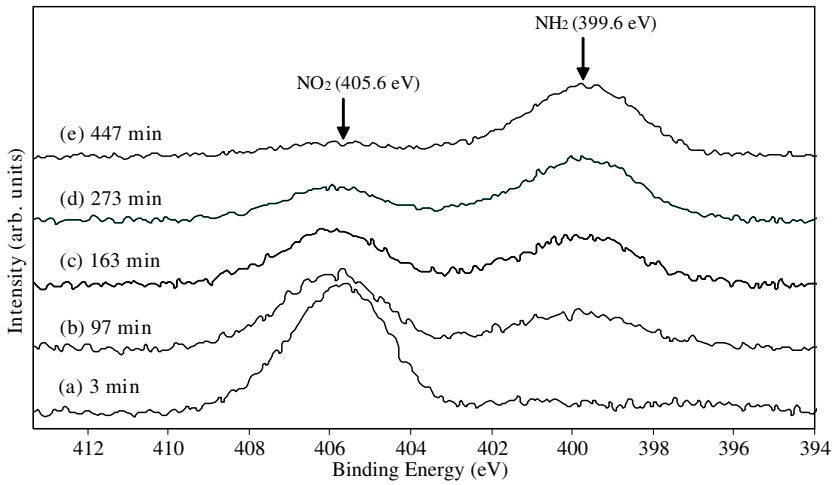

Figure 9. XPS N (1s) spectra of a multilayer film of NPPTMS on Si/SiO_2 taken at 5 time intervals of continuous exposure to x-ray irradiation: after (a) 3 min; (b) 97 min; (c) 163 min; (d) 273 min; (e) 447 min, from [7].

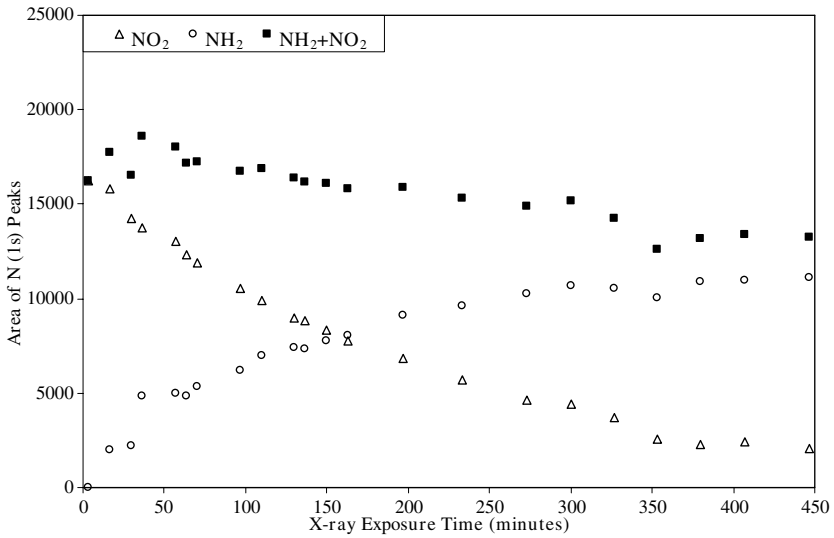

Figure 10. Evolution of the N (1s) peak intensity area for the nitro group (△), amine group (○) and nitro and amine groups (■) during progressive x-ray irradiation, from [7].

Si (2p) peak intensities. These results show that x-ray irradiation could be used for modifying surfaces which contain the NO_2 group to NH_2 functionality. The modified molecular group can be subsequently used for the attachment of gold nanoparticles, which opens up the possibility of functionalizing surfaces in predefined locations or patterns on the nanometre size scale. It is our hope to utilize this system combined with a proximity mask to fabricate amino terminated nanostructures on SiO_2 surfaces to which nanoparticles might assemble from solution, then combining the top-down and bottom-up approach to fabricate nanowires.

6. Outlook

The creation of functionalized nanostructured surfaces is a major challenge. Perhaps of most interest for the future is the possibility of the creation of functional nanostructures by combining the type of bottom-up self-assembling processes, which occur in solution, with top-down lithographic approaches, such as electron beam writing (especially if parallel, rather than serial, lithographic techniques are feasible). The coupling together of such parallel, top-down approaches and bottom-up self-assembly processes suggests that materials and their devices could have multiple length scales, from the micron to the atom.

Acknowledgments

The work described in this article was supported by the European Commission (HPRN-CT-2000-00028) and the EPSRC (GR/N12657/01).

References

[1] Han S W, Lee I and Kim K 2002 *Langmuir* **18** 182–7
Tarlov M J, Burgess D R F Jr and Gillen G 1993 *J. Am. Chem. Soc.* **115** 5305–6
Huang J, Dahlgren D A and Hemminger J C 1994 *Langmuir* **10** 626–8
Chan K C, Kim T, Schoer J K and Crooks R M 1995 *J. Am. Chem. Soc.* **117** 5875–6
[2] Fischer P B and Chou S Y 1993 *Microelectron. Eng.* **21** 311–4
Rangelow I W, Borkowicz Z, Hudek P and Kosti I 1994 *Microelectron. Eng.* **25** 49–66
Despont M, Staufer U, Stebler C, Germann R and Vettiger P 1995 *Microelectron. Eng.* **27** 467–70
[3] Shelley E J, Ryan D, Johnson S R, Couillard M, Fitzmaurice D, Nellist P D, Chen Y, Palmer R E and Preece J A 2002 *Langmuir* **18** 1791–5
[4] Chen Y, Palmer R E, Shelley E J and Preece J A 2002 *Surf. Sci.* **502/503** 208–13
[5] Fitzmaurice D, Rao S N, Preece J A, Stoddart J F, Wenger S and Zaccheroni N 1999 *Angew. Chem., Int. Edn Engl.* **38** 1147–50
[6] Ryan D, Rao S N, Rensmo H, Fitzmaurice D, Preece J A, Wenger S, Stoddart J F and Zaccheroni N 2000 *J. Am. Chem. Soc.* **122** 6252–7
[7] Mendes P, Belloni M, Ashworth M, Hardy C, Nikitin K, Fitzmaurice D, Critchley K, Evans S and Preece J A 2003 *Chem. Phys. Chem.* **41** 884-1
[8] Boal A K, Ilhan F, DeRouchey J E, Thurn-Albrecht T, Russell T P and Rotello V M 2000 *Nature* **404** 746–8
[9] Gittins D I, Bethell D, Schiffrin D J and Nichols R J 2000 *Nature* **408** 67–9
[10] Martin J E, Wilcoxon J P, Odinek J and Prorencio P 2000 *J. Phys. Chem.* B **104** 9475–86
[11] Li M, Schnablegger H and Mann S 1999 *Nature* **402** 393–5
[12] Kiely C J, Fink J, Zheng J G, Brust M, Bethell D and Schiffrin D J 2000 *Adv. Mater.* **12** 640–3
[13] Wang Z L 1998 *Adv. Mater.* **10** 13–30
[14] Zanchet D, Moreno M S and Ugarte D 1999 *Phys. Rev. Lett.* **82** 5277–80
[15] Whetten R L, Shafigullin M N, Khoury J T, Alvarez M M and Wilkinson A 1999 *Acc. Chem. Res.* **32** 397–406
[16] Wang Z L, Harfenist S A, Whetten R L, Bentley J and Evans N D 1998 *J. Phys. Chem.* B **102** 3068–72
[17] Luedtke W D and Landman U 1996 *J. Phys. Chem.* **100** 13323–9
[18] Palmer R E and Guo Q 2002 *Phys. Chem. Chem. Phys.* **4** 4275–84
Chen Y, Palmer R E and Wilcoxon J P 2000 *Surf. Sci.* **454–456** 963–7
Durston P J, Palmer R E and Wilcoxon J P 1998 *Appl. Phys. Lett.* **72** 176–8
Durston P J, Schmidt J, Palmer R E and Wilcoxon J P 1997 *Appl. Phys. Lett.* **71** 2940–2
Osman H, Schmidt J, Svensson K, Palmer R E, Shigeta Y and Wilcoxon J P 2000 *Chem. Phys. Lett.* **330** 1–6
Parker A J, Childs P A, Palmer R E and Brust M 2001 *Nanotechnology* **12** 6–10
[19] Zharnikov M, Frey S, Heister K and Grunze M 2000 *Langmuir* **16** 2697–705
[20] Olsen C and Rowntree P A 1998 *J. Chem. Phys.* **108** 3750–64
[21] Hutt D A and Leggett G J 1999 *J. Mater. Chem.* **9** 923–8
[22] Zharnikov M, Geyer W, Golzhauser A, Frey S and Grunze M 1999 *Phys. Chem. Chem. Phys.* **1** 3163–71
[23] Heister K, Zharnikov M and Grunze M 2001 *Langmuir* **17** 8–11
[24] Service R F 2000 *Science* **290** 1524–31

[25] Welipitiya D, Green A, Woods J P, Dowben P A, Robertson B W, Byun D and Zhang J D 1996 *J. Appl. Phys.* **79** 8730–4
[26] Lavrich D J, Wetterrer S M, Bernasek S L and Scoles G 1998 *J. Phys. Chem.* B **102** 3456–65
[27] Stranick S J, Parikh A N, Tao Y-T, Allara D L and Weiss P S 1994 *J. Phys. Chem.* **98** 7636–46
[28] Troughton E B, Bain C D, Whitesides G M, Nuzzo R G, Allara D L and Porter M D 1988 *Langmuir* **4** 365–85
Takiguchi H, Sato K, Ishida T, Abe K, Yase K and Tamada K 2000 *Langmuir* **16** 1703–10
Jung C, Dannenberger O, Xu Y, Buck M and Grunze M 1998 *Langmuir* **14** 1103–7
Beulen M W J, Huisman B-H, van der Heijden P A, van Veggel F C J M, Simons M G, Biemond E M E F, de Lange P J and Reinhoudt D N 1996 *Langmuir* **12** 6170–2
[29] Lin X M and Sorensen C M 1999 *Chem. Mater.* **11** 198–202
[30] Pankau W M, Verbist K and von Kiedrowski G 2001 *Chem. Commun.* 519–20
[31] Inoue K, Shinkai S, Huskens J and Reinhoudt D N 2001 *J. Mater. Chem.* **11** 1919–23
[32] Brust M, Walker M, Bethell D, Schiffrin D J and Whyman R J 1994 *J. Chem. Soc. Chem. Commun.* 801–2
[33] Ham Y-M, Lee C, Kim S-H and Chun K 1997 *J. Vac. Sci. Technol.* B **15** 2313–7
[34] Fujita J, Ohnishi Y, Manako S, Ochiai Y, Nomura E and Matsui S 1998 *Microelectron. Eng.* **41/42** 323–6
[35] Tada T and Kanayama T 1996 *Japan. J. Appl. Phys.* **35** L63–5
[36] Robinson A P G, Palmer R E, Tada T, Kanayama T, Allen M T, Preece J A and Harris K D M 1999 *J. Phys. D: Appl. Phys.* **32** L75–8
[37] Bedson T R, Palmer R E, Jenkins T E, Hayton D J and Wilcoxon J P 2001 *Appl. Phys. Lett.* **78** 1921–3
Bedson T R, Palmer R E and Wilcoxon J P 2001 *Appl. Phys. Lett.* **78** 2061–3
[38] Jones E T T, Chyan O M and Wrighton M S 1987 *J. Am. Chem. Soc.* **109** 5526–8
[39] He H and Tao N J 2002 *Adv. Mater.* **14** 161–4
[40] Park H, Lim A K L, Alivisatos A P, Park J and McEuen P L 1999 *Appl. Phys. Lett.* **75** 301–3
[41] Miyazaki T, Kobayashi K, Horiuchi T, Yamada H and Matsushige K 2001 *Japan. J. Appl. Phys.* **40** 4365–7
[42] Liu K, Avouris Ph, Bucchignano J, Martel R, Sun S and Michl J 2002 *Appl. Phys. Lett.* **80** 865–7
[43] Chen W and Ahmed H 1993 *Appl. Phys. Lett.* **62** 1499–501
[44] Mccord M A and Rooks M J 1997 *Microlithography in Handbook of Microlithography, Micromaching, and Microfabrication* vol 1, ed P Rai-Choudhury (Bellingham, WA: SPIE Optical Engineering Press and IEE)
[45] Alivisatos A P 1996 *Science* **271** 933–6 and references therein
[46] Murray C B, Norris D J and Bawendi M G 1993 *J. Am. Chem. Soc.* **115** 8706–15
[47] Andres R P, Bielefeld J D, Henderson J I, Janes D B, Kolagunta V R, Kubiak C P, Mahoney W J and Osifchin R G 1996 *Science* **273** 1690–3
[48] Vossmeyer T, Katsikas L, Giersig M, Popovic I G, Diesner K, Chemseddine A, Eychmueller A and Weller H 1994 *J. Phys. Chem.* **98** 7665–73
[49] Harfenist S A, Wang Z L, Alvarez M A, Vezmar I and Whetten R L 1996 *J. Phys. Chem.* **100** 13904–10
[50] Herron N, Calabrese J C, Farneth W E and Wang Y 1993 *Science* **259** 1426–8
[51] Schmid G 1992 *Chem. Rev.* **92** 1709–27
[52] Moritz T, Reiss K, Diesner K, Su D and Chemseddine A 1997 *J. Phys. Chem.* B **101** 8052–3
[53] Brus L 1986 *J. Phys. Chem.* **90** 2555–60
[54] Murray C B, Kagan C R and Bawendi M G 1995 *Science* **270** 1335–8
[55] Kagan C R, Murray C B and Bawendi M G 1996 *Phys. Rev.* B **54** 8633–43
[56] Heath J R, Knobler C M and Leff D V 1997 *J. Phys. Chem.* B **101** 189–97
[57] Motte L, Billoudet F, Lacaze E, Douin J and Pileni M-P 1997 *J. Phys. Chem.* B **101** 138–44
[58] Bentzon M D, vanWonterghem J, Morup S and Tholen A 1989 *Phil. Mag.* B **60** 169–75
[59] Sellers H, Ulman A, Shnidman Y and Eilers J E 1993 *J. Am. Chem. Soc.* **115** 9389–401
[60] Badia A, Singh S, Demers L, Cuccia L, Brown G R and Lennox R B 1996 *Chem. Eur. J.* **2** 359–63
[61] Hostetler M J, Green S J, Stokes J J and Murray R W 1996 *J. Am. Chem. Soc.* **118** 4212–3
Ingram R S, Hostetler M J and Murray R W 1997 *J. Am. Chem. Soc.* **119** 9175–8
Templeton A C, Hostetler M J, Warmoth E K, Chen S, Hartshorn C M, Krishnamurthy V M, Forbes M D E and Murray R W 1998 *J. Am. Chem. Soc.* **120** 4845–9
[62] Ulman A 1989 *J. Mater. Ed.* **11** 205–79
Sellers H, Ulman A, Shnidman Y and Eilers J 1993 *J. Am. Chem. Soc.* **115** 9389–401
[63] Weitz D and Oliveria M 1984 *Phys. Rev. Lett.* **52** 1433–6
Weitz D, Huang J, Lin M and Sung J 1984 *Phys. Rev. Lett.* **53** 1657–60
Weitz D, Huang J, Lin M and Sung J 1985 *Phys. Rev. Lett.* **54** 1416–9
Zhou Z and Chu B 1991 *J. Colloid Sci.* **143** 356–65
Zhou Z, Wu P and Chu B 1991 *J. Colloid Sci.* **146** 541–55
[64] Janos H F 2001 *Chem. Mater.* **13** 3196–210

[65] Han S W, Lee I and Kim K 2002 *Langmuir* **18** 182–7
[66] He H X, Zhang H, Li Q G, Zhu T, Li S F Y and Liu Z F 2000 *Langmuir* **16** 3846–51
Yan L, Huck W T S, Zhao X-M and Whitesides G M 1999 *Langmuir* **15** 1208–14
Xia Y and Whitesides G M 1998 *Angew. Chem., Int. Edn Engl.* **37** 550–75
[67] Weimann T, Geyer W, Hinze P, Volker S, Eck W and Gölzhäuser A 2001 *Microelectron. Eng.* **57/58** 903–7
[68] Piner R D, Zhu J, Xy F, Hong S and Mirkin C A 1999 *Science* **283** 661–3
Hong S, Zhu J and Mirkin C A 1999 *Science* **286** 523–5
[69] Liu G Y, Xu S and Qian Y L 2000 *Acc. Chem. Res.* **33** 457–73
Xu S and Liu G-Y 1997 *Langmuir* **13** 127–9
[70] Yang X M, Peters R D, Kim T K, Nealey P F, Brandow S L, Chen M-S, Shirley L M and Dressick W K 2001 *Langmuir* **17** 228–33
[71] Eck W, Stadler V, Geyer W, Zharnikov M, Gölzhäuser A and Grunze M 2000 *Adv. Mater.* **12** 805–8
[72] Ulman A 1991 *An Introduction to Ultrathin Organic Films* (London: Academic)
[73] Ulman A 1996 *Chem. Rev.* **95** 1533–54
[74] Wagner A J, Han K, Vaught A L and Fairbrother D H 2000 *J. Phys. Chem.* B **104** 3291–7
Heister K, Zharnikov M, Grunze M, Johansson L S O and Ulman A 2001 *Langmuir* **17** 8–11
[75] Rieke P C, Baer D R, Fryxell G E, Engelhard M H and Porter M S 1993 *J. Vac. Sci. Technol.* A **11** 2292–7
[76] Frydman E, Cohen H, Maoz R and Sagiv J 1997 *Langmuir* **13** 5089–106
[77] Moon J H, Kim K-J, Kang T-H, Kim B, Kang H and Park J W 1998 *Langmuir* **14** 5673–5
[78] La Y-H, Kim H J, Maeng I S, Jung Y J and Park J W 2002 *Langmuir* **18** 301–3
[79] La Y-H, Kim H J, Maeng I S, Jung Y J and Park J W 2002 *Langmuir* **18** 2430–3
[80] Laibinis P E, Graham R L, Biebuyck H A and Whitesides G M 1991 *Science* **254** 981–3
[81] Zharnikov M and Grunze M 2002 *J. Vac. Sci. Technol.* B **20** 1793–807
[82] Briggs D and Seah M P 1996 *Practical Surface Analysis* (Chichester: Wiley)
[83] Nielsen J U, Espandiu M J and Kolb D M 2001 *Langmuir* **17** 3454–9